1   **Airflow dynamics, vegetation and aeolian erosive processes in a shadow zone leeward of a**

2   **resort in an arid transgressive dune system**

3

4   ABSTRACT

5   Structures and infrastructures can modify aeolian sedimentary dynamics as has occurred in

6   the arid transgressive dunefield of Maspalomas (Gran Canaria, Canary Islands), where an aeolian

7   shadow zone has been formed leeward of a tourist resort (Playa del Inglés). The aim of this paper

8   is to examine and statistically analyse the influences of vegetation and topography on wind

9   flow across this shadow zone. An experiment was carried out in March 2017, collecting wind speed

10   and direction from 5 transects with anemometers at 0.40 m height. Simultaneously, a drone flight was

11   carried out, from which an orthophoto and digital elevation and surface models (DEM and DSM)

12   were obtained. Distance from the resort, and the presence of vegetation were found to influence

13   transects dominated by erosional processes. Transects that do not display erosional processes were

14   primarily affected by the presence of vegetation. The local wind field changes at a similar distance

15   across the transects downwind from the resorts indicating an acceleration or reattachment of the wind

16   at this distance downwind. The vegetation role in this aeolian shadow zone could be a key to the

17   future evolution of the area resulting in either further stabilization, or alternatively, the continued

18   deflation of the area.

19   Keywords: aeolian shadow zone, arid transgressive dune system, wind flow, dune vegetation,

20   topography, human impact.

21

22   **1. Introduction**

23   Coastal dune systems have been significantly altered in the Anthropocene, which is

24   characterized by the modification of natural processes due to human development (Crutzen and

25   Stoermer, 2000), especially in recent decades (Nordstrom, 2004; Jackson and Nordstrom, 2011). Arid

coastal dune systems of the Canary Islands constitute a clear example of this process. Their mild climate has attracted millions of tourists over the last decades, and urban-tourist buildings around these systems are producing significant environmental changes (Hernández-Calvento et al., 2014; García-Romero et al., 2016; Hernández-Cordero et al., 2017).

The urban-tourist occupation induces alterations in the natural processes of coastal dune systems, the greatest of which are related to geomorphological and vegetation changes (Cabrera-Vega et al., 2013; Hernández-Calvento et al., 2014; García-Romero et al., 2016; Hernández-Cordero et al., 2017; García-Romero et al., 2019). When buildings or infrastructure are located near or inside dune fields they act as rigid and impermeable structures that intrude upon and modify the regional wind flow and local Internal Boundary Layer (IBL), and alter aeolian sediment dynamics (Nordstrom and McCluskey, 1984; Gundlach and Siah, 1987; Nordstrom and Jackson, 1998; Tsoar and Blumberg, 2002; Wiedemann and Pickart, 2004). Although many natural and anthropogenic factors influence dunefield mobility, the direct interaction between urbanization and physical processes remains largely unexplored (Nordstrom, 1994; Jackson and Nordstrom, 2011). To address this lack of studies, pioneering research on the direct impact of urban-tourist buildings on dune systems has been developed in Maspalomas dune field (Gran Canaria) within the last few years, specifically on changes to airflow dynamics. Hernández-Calvento et al. (2014) developed a simplified numerical wind model based on a logarithmic wind velocity profile, and Smith et al. (2017) investigated regional airflow modeling during successive stages of urbanization using Computational Fluid Dynamic (CFD) modelling. These studies have allowed exploration of how the resort development on a high terrace overlooking the dunefield has modified the aeolian sedimentary dynamics in this dune system (Hernández-Calvento et al., 2014, Smith et al., 2017).

Regional disturbances of the air flow due to the development of the resorts gave rise to three geomorphological zones, namely, an acceleration zone south of the terrace, and two deceleration zones with different degrees of sedimentary stabilization and an increase in plant cover in the west (Hernández-Cordero et al., 2017). One of these deceleration zones was characterized by García-

52 Romero et al. (2019) based on its biogeomorphological processes (Figure 1, study plot). Two

53 processes were identified in the aeolian shadow zone (leeward of the terrace): a progressive

54 sedimentary deficit, and the increase in vegetation density. Also, three erosional aeolian landforms,

55 located at a distance of about 400-500 meters from the resort, are expanding. These erosional

56 landforms are the result of wind acceleration at a local scale resulting from the interaction of the

57 buildings on the airflow (García-Romero et al., 2017; 2019). Mir-Gual et al. (2015) speculated that

58 streets between the buildings on top of El Inglés terrace can act as wind corridors that channel the

59 airflow, locally increasing wind speed in the shadow zone and generating these three erosional

60 landforms. In fact, these processes do not occur in areas behind taller buildings (Mir-Gual et al.,

61 2015). The increase in size and area covered by these erosional landforms, resulting in exhumed roots

62 of herbaceous plants, is a direct consequence of blocking sediment transport following the completion

63 of the urbanization on top of the terrace (García-Romero et al. 2019). As suggested, it is possible to

64 argue that a large deflation landform will dominate in this area in the future rather than stabilized

65 landforms (Hernández-Calvento et al., 2014; Hernández-Cordero et al., 2015), which could depend

66 on the functioning and evolution of shrub vegetation (García-Romero et al. 2019). New studies are

67 therefore required to characterize aeolian processes in this area at a local scale, including the

68 relationship between wind flow and environmental variables, such as topography and vegetation, as

69 well as the distances from the resort.

70   The aim of this study is to characterize and analyze aeolian processes in the aeolian shadow

71 zone of the Playa del Inglés resort, and to relate local wind flows to topography, vegetation and

72 distance to buildings. This follows previous suggestions by Garcia-Romero et al. (2019) who

73 highlighted the need to acquire high temporal and spatial resolution wind records in this area to allow

74 detailed quantification of airflow processes involved in the evolution of this erosional and/or

75 stabilizing landscape, as well as to identify the reasons for the erosional landforms on similar

76 distances downwind of the buildings.

77

78   **2. Material and methods**

79   *2.1. Study area*

80   The arid transgressive dune system of Maspalomas (360.9 ha.) is located on the south of Gran

81   Canaria (figure 1), on a fan-delta. Effective winds and the predominant aeolian sediment transport,

82   are ENE-WSW (Máyer-Suárez et al., 2012). The sediment enters the dune system by the eastern

83   beach (El Inglés) and is transported toward the southern beach (Maspalomas), where it returns to the

84   sea. A Pleistocene high wedge-shaped terrace (about 25 meters above sea level (m.a.s.l.)) on the

85   north-eastern boundary interacts with the wind flow and the sedimentary transport. Construction on

86   this terrace from the 1960s resulted in one of the largest tourist resorts in Spain (Domínguez-Mujica

87   et al., 2011). The urban-tourist resort has a strong impact on aeolian processes, altering the wind flow

88   and therefore the sediment transport, and generating different processes resulting in the three

89   geomorphological areas described in section 1 (Hernández-Calvento et al., 2014, Smith et al., 2017;

90   Hernández-Cordero et al., 2017). In this work we focus on the aeolian shadow zone, located leeward

91   of the tourist resort (see area C in the study plot, Figure 1).

92
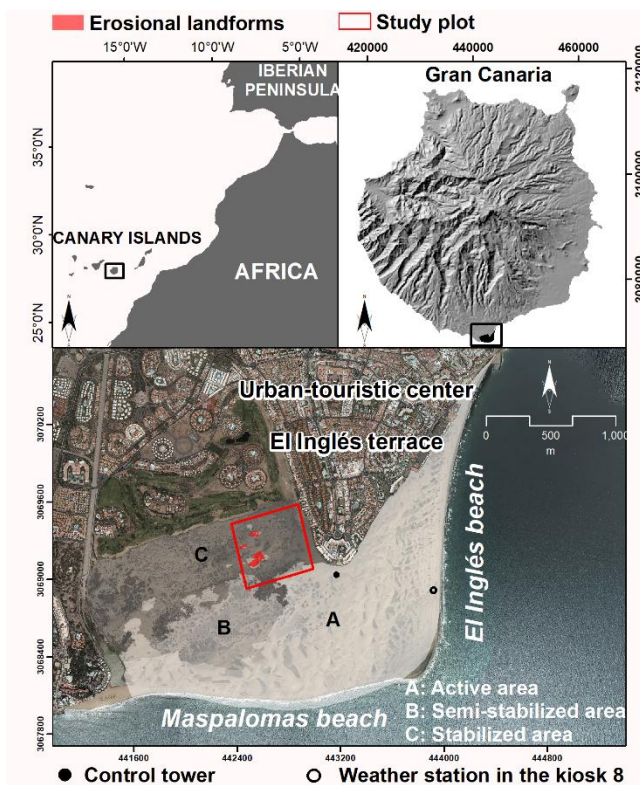
Figure 1. Arid transgressive dune system of Maspalomas, with the study plot (red box), erosional landforms (in red) and location of two wind sensors for determining local wind data. A (area of airflow acceleration), B and C (areas of airflow deceleration), as defined by Hernández-Cordero et al (2015).

A study plot of 27.76 hectares was delimited leeward and westward of the tourist resort, where the data were collected (figure 2). The experiment was conducted on 24th and 25th March 2017, consisting of simultaneous capture of wind, topography and vegetation characteristics. Distances to the resort were measured using geographical information system (GIS) tools. Plant communities data inside the erosional landforms were collected to explain the role of vegetation in this zone.
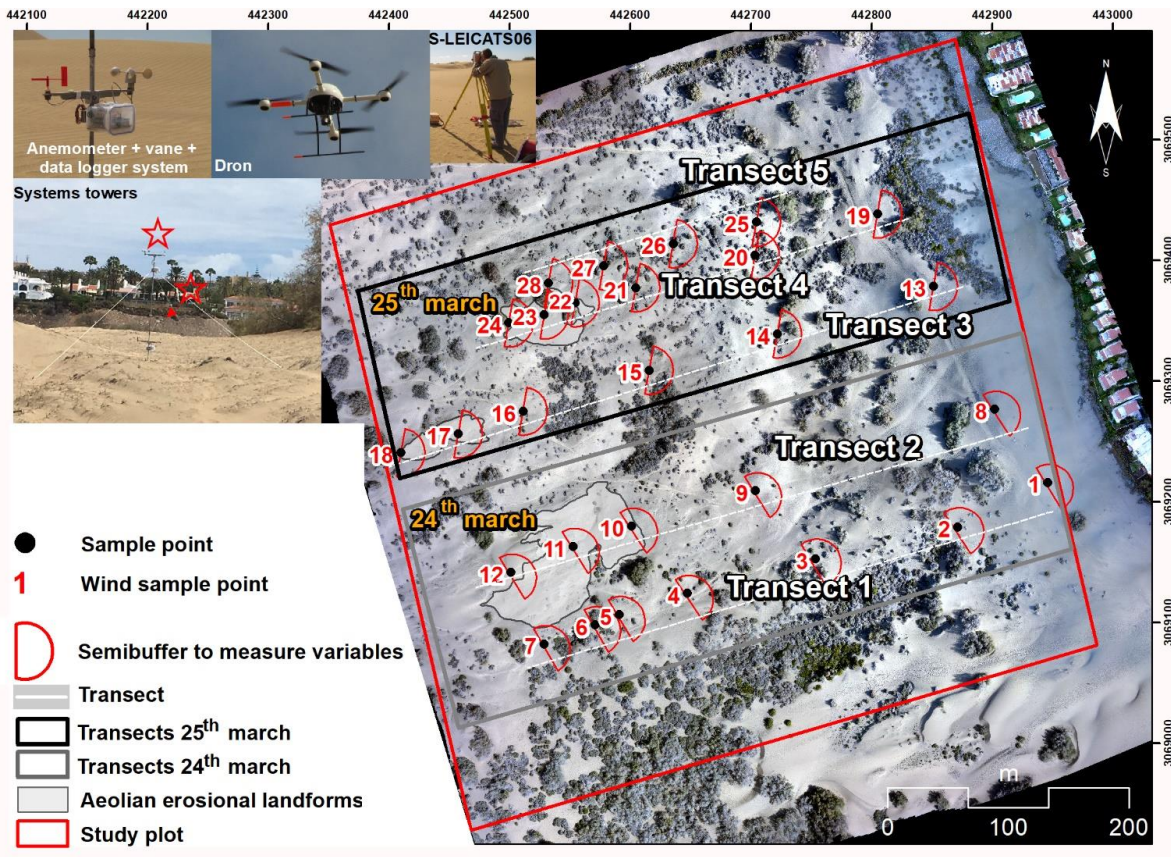
Figure 2. Transects and wind sampling points on March 24th and 25th, 2017. Transects 1 and 5 were outside the aeolian erosional landforms area, and transects 2, 3 and 4 were inside the area. The

106   semibuffer (red) with a radius of 20 meters indicates areas where other environmental variables

107   (vegetation and topography) were measured.

108

109   *2.2. Wind data*

110   Airflow data were collected by 10 mobile wind stations with wireless communication. The

111   stations consisted of an anemometer-vane-data logger system and were deployed in towers at two

112   different heights: at 0.4 m height above the surface (data presented in this paper) and at 2.10 m above

113   the surface (figure 2). The inclusion of two wind stations per tower reduced to 5 the number of

114   locations that could be sampled simultaneously but provided synchronous information on the

115   dynamics of the local airflow at 2.10 m height, and on the dynamics of near-surface airflow (where

116   most sediment transport occurs). This allowed the possibility to know if these airflows are affected

117   by the resorts and at the same time also influenced by vegetation or topography. Sampling at all

118   locations was completed by moving four towers sequentially, while the fifth (control tower) remained

119   in a fixed position, outside the wind shadow zone (figure 1). A total of 5 transects were completed

120   from 28 sample points (figure 2) across areas with and without observed sediment erosion processes,

121   as well as near the vegetation, allowing complete cover of the shadow zone and ensuring that all data

122   could be collected within the same experiment. The transects were strategically located to measure

123   airflow around and inside erosional landforms, and in front and behind vegetation and in the

124   topographic lows and highs. The order to collect the data was from the simultaneous sample Run 1

125   (figure 5. wind sample points 1-4) closer to the control tower (figure 1), Run 2 (figure 5. wind sample

126   points 5-8), Run 3 (figure 5. wind sample points 9-12), Run 4 (figure 6. wind sample points 13-16),

127   Run 5 (figure 6. wind sample points 17-20), Run 6 (figure 6. wind sample points 21-24), to the Run

128   7 (figure 6. wind sample points 25-28). Additionally, wind data were collected every 10 minutes at a

129   station located on a beach kiosk, at 4 m height, on El Inglés beach (figure 1). Data were collected at

130   each location for 40 minutes. The regional wind direction varied during the data collection period.

131   Following previous studies (Delgado-Fernández et al., 2013), wind records were filtered by wind

132   direction, specifically between 40° and 70° on the 24th and between 70° and 100° on the 25th of

133   March. These ranges were calculated from the data collected at the El Inglés beach stations and the

134   control tower (Figure 3). This allowed the isolation of periods of time in all stations during which the

135   incident wind direction was similar, with changes in wind characteristics between stations due to a

136   range of other variables including topographic factors, vegetation, and distance to the resort.
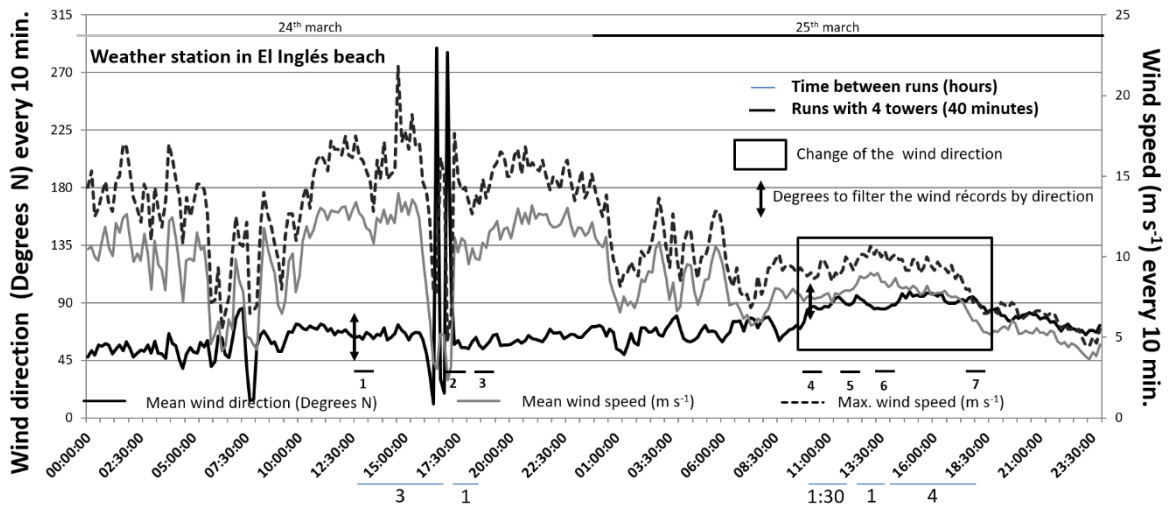
137

138   Figure 3. Wind conditions at El Ingles beach weather station (Kiosk 8). The graph shows the entire

139   data set (every 10 minutes) recorded at the beach station during the experiment, the simultaneous

140   wind sampling with 4 towers (Runs 1-7), and the change of wind direction between both days

141   (black square).

142

143   In Table 1, standard deviations (m/s^{-1}) are shown to explain the errors of the mean wind speed

144   which are indicated in figures 5 and 6 in each run. In general, the standard deviations have a low

7

145 significance with respect to the wind speeds collected. The biggest standard deviations occured in

146 the first 2 runs, especially in the minutes 10, 15, 25, 30 and 40 when the wind speed is constantly

147 changing.

148

149 Table 1. Standard deviations of the mean in every 5 minute timeslot (Figure 5 and 6) to show the

150 errors (m/s^{-1}) in the wind speeds analyzed.

Run	Wind sample point	wsmin5	wsmin10	wsmin15	wsmin20	wsmin25	wsmin30	wsmin35	wsmin40
	Control	0.335	0.375	0.521	0.327	0.746	0.399	0.295	0.218
	1	0.354	0.497	0.432	0.371	0.578	0.408	0.582	0.493
1	2	0.309	0.33	0.322	0.292	0.558	0.467	0.52	0.401
	3	0.353	0.325	0.3	0.372	0.519	0.491	0.514	0.408
	4	0.323	0.348	0.231	0.272	0.529	0.47	0.364	0.368
	Control	0.379	0.432	0.294	0.236	0.859	0.493	0.486	0.495
	5	0.467	0.455	0.326	0.371	0.081	0.361	0.243	0.299
2	6	0.434	0.411	0.343	0.142	0.189	0.208	0.177	0.072
	7	0.159	0.044	0.107	0.202	0.094	0.42	0.079	0.083
	8	0.456	0.419	0.398	0.23	0.27	0.182	0.245	0.144
	Control	0.217	0.421	0.389	0.316	0.247	0.262	0.326	0.283
	9	0.236	0.207	0.384	0.203	0.34	0.259	0.313	0.272
3	10	0.155	0.274	0.368	0.308	0.19	0.238	0.331	0.222
	11	0.178	0.222	0.4	0.365	0.244	0.208	0.305	0.267
	12	0.258	0.381	0.446	0.348	0.335	0.303	0.314	0.329
	Control	0.279	0.289	0.271	0.252	0.383	0.242	0.232	0.257
	13	0.309	0.317	0.338	0.236	0.592	0.269	0.266	0.348
4	14	0.308	0.31	0.297	0.324	0.398	0.365	0.231	0.304
	15	0.2	0.144	0.228	0.23	0.203	0.172	0.175	0.209
	16	0.339	0.426	0.261	0.259	0.38	0.201	0.216	0.208
	Control	0.232	0.148	0.228	0.251	0.223	0.224	0.245	0.220
	17	0.291	0.16	0.283	0.374	0.313	0.265	0.308	0.349
5	18	0.255	0.094	0.254	0.216	0.189	0.25	0.271	0.23
	19	0.143	0.168	0.194	0.202	0.221	0.178	0.207	0.136
	20	0.24	0.169	0.182	0.212	0.168	0.204	0.193	0.163
6	Control	0.261	0.256	0.257	0.264	0.337	0.290	0.351	0.437

	21	0.243	0.287	0.259	0.254	0.308	0.327	0.379	0.479
	22	0.216	0.194	0.189	0.228	0.342	0.359	0.348	0.394
	23	0.378	0.319	0.344	0.297	0.398	0.24	0.328	0.453
	24	0.168	0.182	0.197	0.195	0.259	0.193	0.31	0.38
	Control	0.253	0.243	0.247	0.233	0.380	0.348	0.421	0.337
	25	0.368	0.365	0.362	0.296	0.438	0.341	0.408	0.354
7	26	0.179	0.295	0.26	0.211	0.49	0.364	0.438	0.355
	27	0.221	0.206	0.24	0.242	0.414	0.324	0.486	0.362
	28	0.283	0.144	0.164	0.184	0.217	0.324	0.39	0.237

151

152   The anemometer-vane-data logger systems to collect the wind data (figure 4) are wireless

153   devices (figure 4A) that measure wind characteristics (direction and speed). All instruments store

154   measurements in their data loggers, which are synchronized with other devices. A software

155   specifically designed for this application controls and executes measurement options from the base

156   station (figure 4A and 4B). The base station also communicates wirelessly with the rest of the sensors

157   and controls the correct functioning of the entire grid in real time.

158
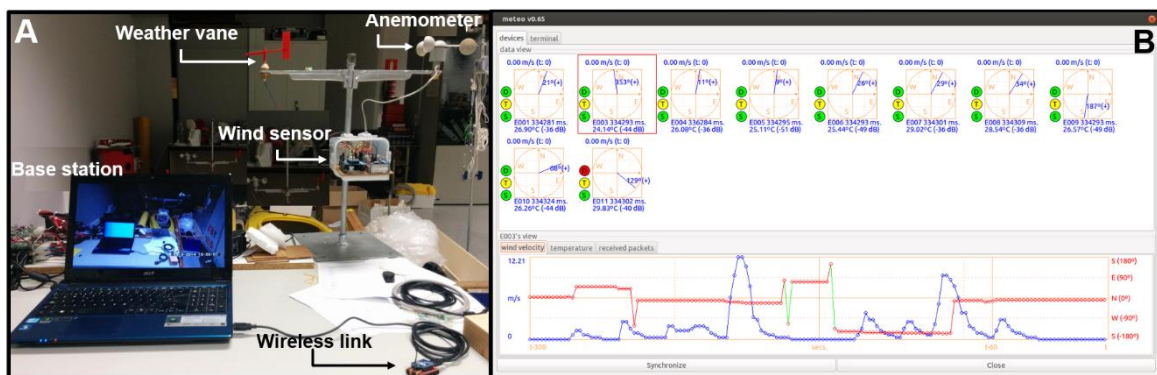
159

160   Figure 4. Characteristics of the wind sensors. A. Base station with wireless link (Xbee) to connect

161   with the wind-vane + anemometer + data logger system. B. Software developed to check and

162   synchronize the wind sensors in an experiment with 10 wind sensor systems. The data of the second

163   wind sensor system (orange square) can be observed in the graphics.

9

164

165   Wind speed and direction were averaged every five minutes with the purpose of ensuring a

166 sufficient time of observation and to guarantee that the entire area was affected by the same wind

167 flow over a given period. Each average speed (m s^{-1}) of 5 minutes duration in the towers (*ASP*) was

168 normalized with respect to the average corresponding to the control tower of the same simultaneous

169 sampling (*ACT*) (Delgado-Fernández et al., 2013). This normalization (*WN*) was carried out in order

170 to eliminate the differences in wind speed changes during the experiment due to changes in the

171 position of the wind sampling points to cover the transect completely, and thus be able to compare

172 the data taken in the same day (equation 1). Figures 5 and 6 show these results stored in a shapefile

173 with point geometry, where the average direction is shown by rotation and the speed normalized from

174 the size of the chosen symbology.

175 $$WN = ASP/ACT \tag{1}$$

176 where *WN* is the wind speed normalized and shown in the results (figure 5 and 6, left), *ASP* is the

177 wind speed taken at each sample point inside the study plot (figure 2), and *ACP* is the wind speed

178 taken at the control tower (figure 1).

179 *2.3. Topography and vegetation*

180   For each wind sampling point, a semibuffer with a radius of 20 m distance was established

181 oriented into the predominant wind direction (figure 2) through GIS vectors (polygon) digitalitation.

182 This distance was defined by Alonso-Bilbao et al. (2007) as the distance along which the wind flow

183 is influenced by a plant obstacle of the shrub species *Traganum moquinii* in Maspalomas.

184 Topographic and vegetation variables were measured inside this semibuffer using a digital orthophoto

185 (spatial resolution of 0.05 m) from a photogrammetric drone flight carried out on March 25th, 2017.

186 The point mesh was used to derive topographic information (in .las format). The precision of the data

187 was tested using ground data collected with a Leica TS06 total station with laser device. For the

188 topographic information, algorithms were applied to detect occlusions (Chang et al., 2008), deriving

189 a digital elevation model (DEM) and a digital surface model (DSM). The average degree of slope and

190 the average altitude of the surface inside the semibuffers were calculated using basic algorithms

191 implemented in GIS on the MDE. The vegetation variables calculated were the mean vegetation

192 density and the maximum vegetation height in each semibuffer. The first one was calculated applying

193 the procedure developed by Garcia-Romero et al. (2018), making use of the orthophoto obtained by

194 the drone flight. The maximum vegetation height was extracted from the MDS. The vegetation cover

195 shown in the figure 8 to relate distance to the urbanization and the distribution of the vegetation was

196 calculated through GIS reclassification using the same orthophoto, the areas every 100 m were

197 calculated through proximity GIS tools and the spatial analysis using overlay tools. The plant

198 communities data for the year 2003 were obtained from Hernández-Cordero et al. (2017). The

199 vegetation data of 2017 were obtained from Garcia-Romero et al. (2019). Both data were developed

200 through visual interpretation of digital orthophotos (using variables such as color, size, density,

201 texture and spatial pattern) and supported by field work.

202

203 *Distance to the urbanization*

204   Distances between individual wind stations and the resort were measured through algorithms

205 implemented in GIS, calculating the closest distance between vector layers: a point geometries layer

206 representing each wind station and a polygon geometry representing the resort.

207 *2.4. Principal Components Analysis*

208	Principal Component Analyses (PCA) was used to explore a first statistical approximation of

209	what variables measured in the semibuffers best represent each transect. A series of components and

210	the significance of the variables that best represent each transect were obtained. To achieve a more

211	robust analysis, we use the normalized winds shown in figure 5 and 6 (for the averages 20 and 30

212	minutes in transects 1-2 and 3-5 respectively) because these time periods show greater similarity to

213	the higher wind speeds recorded. In addition, the same analysis was also done with the average

214	centered around minutes 5 and 10 for transects 1-2 and 3-5 respectively, because they show greater

215	similarity than the previous ones, although with lower speeds, especially in transects 1 and 2. From

216	transect 1 to transect 4 (averages of minutes 20 and 30), only the first and second component were

217	obtained because they explain 84.9%, 88.41%, 90.6%, 97.58% respectively of the variance, except

218	transect 5 (average centered in minute 30) where the first component explains 96.61% of the variance.

219	In the same way, the first and second components explain the 81.9%, 88.5%, 85.7%, 92.7% of the

220	variance in the averages centered around minutes 10 and 5 (transects 1-4) and the first component in

221	the transect 5 (minute 5) explains 96.7% of the variance. Finally the relationship between the variable

222	with greater significance in the first component and the wind data (speed m s^{-1}), at normalized scale,

223	was analyzed. These relationships are shown by dispersion diagrams, adjusted with second order

224	polynomial except the distance to urbanization in transects 2 and 3 that were adjusted with third order

225	polynomial. These graphics illustrate the behavior (when and where) of the wind speed (acceleration

226	or deceleration) with respect to the environmental variables measured.

227

228	**3. Results and discussion**

229	*3.1.Wind data and aeolian processes*

12

230   Figure 5 (C, Run 1-3) shows the temporal variability of wind speeds ($m\ s^{-1}$) collected at each

231   sampling location and in the control tower every 5 minutes on March 24th, 2017. In Run 1, wind

232   speeds at points 1 and 2 (closer to the resort) were slower than those recorded at points 3 and 4 (further

233   away from the resort). The trend showed some temporal variability: on average, centered around

234   minute 25, winds were similar at all points, while, on average, centered on minute 35, the areas closest

235   to the urbanization had higher wind speeds as a result of a change in wind direction closer to 70°

236   (Figure 3, Run 1), which produce more obliquity on wind toward the aeolian shadow zone, and the

237   wind can penetrate this area more directly and strongly. With respect to the control tower, the wind

238   speeds were significantly higher until the average of minute 25, where the shadow effect practically

239   disappeared. Also, in the average centered in minute 35 the sampling point closest to the urbanizations

240   (1) had a faster wind speed than the control tower, which could be explained because of a change in

241   wind direction and the possible urban obstacle that generated accelerations within the wind shadow

242   area. This behavior is similar to that explained previously, that is, the wind direction near to 70°

243   displays higher obliquity and accelerates the winds towards the area with the greater aeolian shadow

244   because they penetrate more directly. In terms of points 5 to 8 (Run 2), and similar to the previous

245   transect, locations furthest away from the resort (6 and 7) showed fast wind speeds compared to those

246   closest to the resort, with changes to this trend found in averages centered in the minutes 20, 25 and

247   35. The control tower presented significant differences in wind speeds (faster) with respect to the

248   sampling points. Finally, in terms of points 9 to 12 (Run 3), although the control tower collected faster

249   wind speeds, the difference was not significant. Wind speeds between sampling locations did not

250   show clear differences either, although point 35 (at a greater distance from the resort) recorded faster

251   wind speeds.

252   For the purpose of analyzing spatial patterns in wind data collected at all sampling locations,

253   (Figure 5, A and B), the average centered on minute 20 of all runs was selected because of relatively

254   strong wind speeds and because winds collected by the control tower were similar (black circle in the

255   wind time series of Figure 5, C). Also, because higher speeds can produce greater erosional processes

256   if this occurs inside the study plot. In general, winds accelerated away from the resort. However, in

257   transect 1 (figures 2 and 4, sampling points 1-7), winds were reduced in the last three sampling points,

258   coinciding with the presence of vegetation, especially shrubby plants (figure 7 profile of the transect

259   1). This increased the roughness of the terrain and reduced both wind speed and sedimentary transport

260   (Hesp, 1981; Moreno-Casasola, 1986). In transect 2 (figures 2 and 5 sample points 8-12), there was

261   only a negligible drop in the wind speed of the points located within an erosional landform, which

262   may be caused by the topographic features or by the roughness of the vegetation (Hesp, 1981;

263   Moreno-Casasola, 1986), especially and currently the herbaceous plant community *Cyperus*

264   *capitatus-Ononis serrata* (table 3). This also happened at the beginning of the transect, which can be

265   explained by the shadow effect of the resort (Hernández-Calvento et al., 2014, Smith et al., 2017).

14
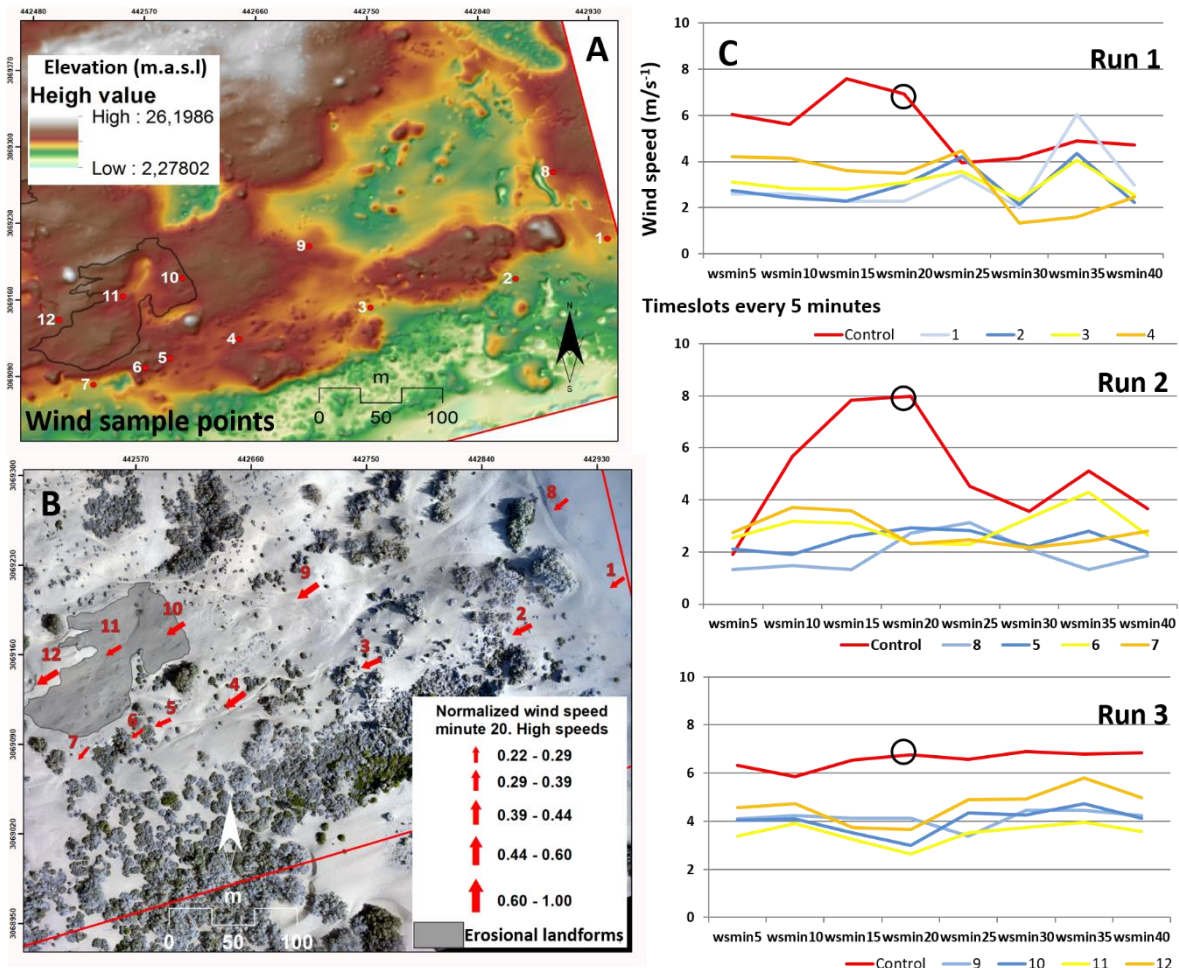
Figure 5. (A) Position of the sampling points. (B) results of the normalized wind speed (ASP/ACT) (minute 20, black circle of the Run`s graphs) with respect to the control tower in each simultaneous sampling. (C) Wind speeds (m s^{-1}), average every 5 minutes in the sampling points on March 24th, 2017 (right, Run 1-3).

In terms of the data obtained on March 25th, 2017 (Figure 6, C), a reduction in wind speed was observed closest to the resort between the sampling points 13 and 16 (Run 4). Wind speeds increased as the distance from the resort increased (e.g., point 16) and were higher than at the control

15

275 tower. A similar trend is observed between points 17 and 20 (Run 5), although wind speeds at

276 locations farthest away from the resort did not exceed those recorded by the control tower.

277 There were no significant differences between points 21 and 24 in Run 6 (ranging from 3 to

278 4 m s^{-1}), although point 21, the closest to the resort, registered the highest wind speeds, except for the

279 average centered on minute 30, when all points record similar speeds, but still exceeding those

280 recorded by the control tower.

281 Finally, in Run 7, points 25, 26 and 27 showed similar wind speeds at all times. Point 28, at

282 a greater distance from the resort, registered higher wind speeds than the control tower. Similar to

283 Figure 5, normalized wind speeds were plotted at all instrument locations (Figure 6, A and B) for the

284 average centered on minute 30 (black circle in Figure 6, C) coinciding with the lowest differences in

285 wind speeds in the control tower. The wind, again, accelerated as it moved away from the resort,

286 regardless of the presence of erosional landforms. In transect 3 (figure 2 and 6, sampling points 13-

287 18), a wind speed reduction was observed at the first two points (13 and 14). In relation to the first

288 one, this could be explained by the shadow effect of the resort, as detected by Hernández-Calvento et

289 al. (2014) and Smith et al. (2017). In relation to the second one, it could be due to the presence of

290 vegetation, as in the aforementioned case. From this location, the wind accelerated constantly,

291 although within the erosional landform there was a setback that could be explained by the topographic

292 features, which slowed the wind slightly because it is a trough blowout (Hesp, 2002), or by the

293 presence of vegetation due to the roughness of the terrain that can reduce the wind speed and sediment

294 transport (Mayaud et al., 2017). In the latest case, there was only a herbaceous plant community

295 (*Cyperus capitatus-Ononis serrata,* Table 3) between 2003 and 2017 according to Hernández-

296 Cordero et al. (2017) and Garcia-Romero et al. (2019). Transect 4 (figure 2 and 6, sample points 19-

297 24) had constant wind speeds likely regulated by vegetation (Mayaud et al, 2016), similar to transect

298   1 where there was shrubby vegetation at the beginning of the transect (Figure 6, profile of the transect

299   4). In this case, the vegetation detected inside the erosional landform was the herbaceous plant

300   community *Cyperus capitatus-Ononis serrata* and null or low vegetation (table 3).

301   There were no erosional landforms along transect 5 (figure 2 and 6, sample points 25-28).

302   Wind speeds recorded at the first points along this transect were affected by shrubby vegetation

303   (figure 7, A. profile of the transect 5), similar to transects 1 and 4. Wind speeds significantly

304   accelerated at the last point coinciding with the erosional landform of transect 4.

305
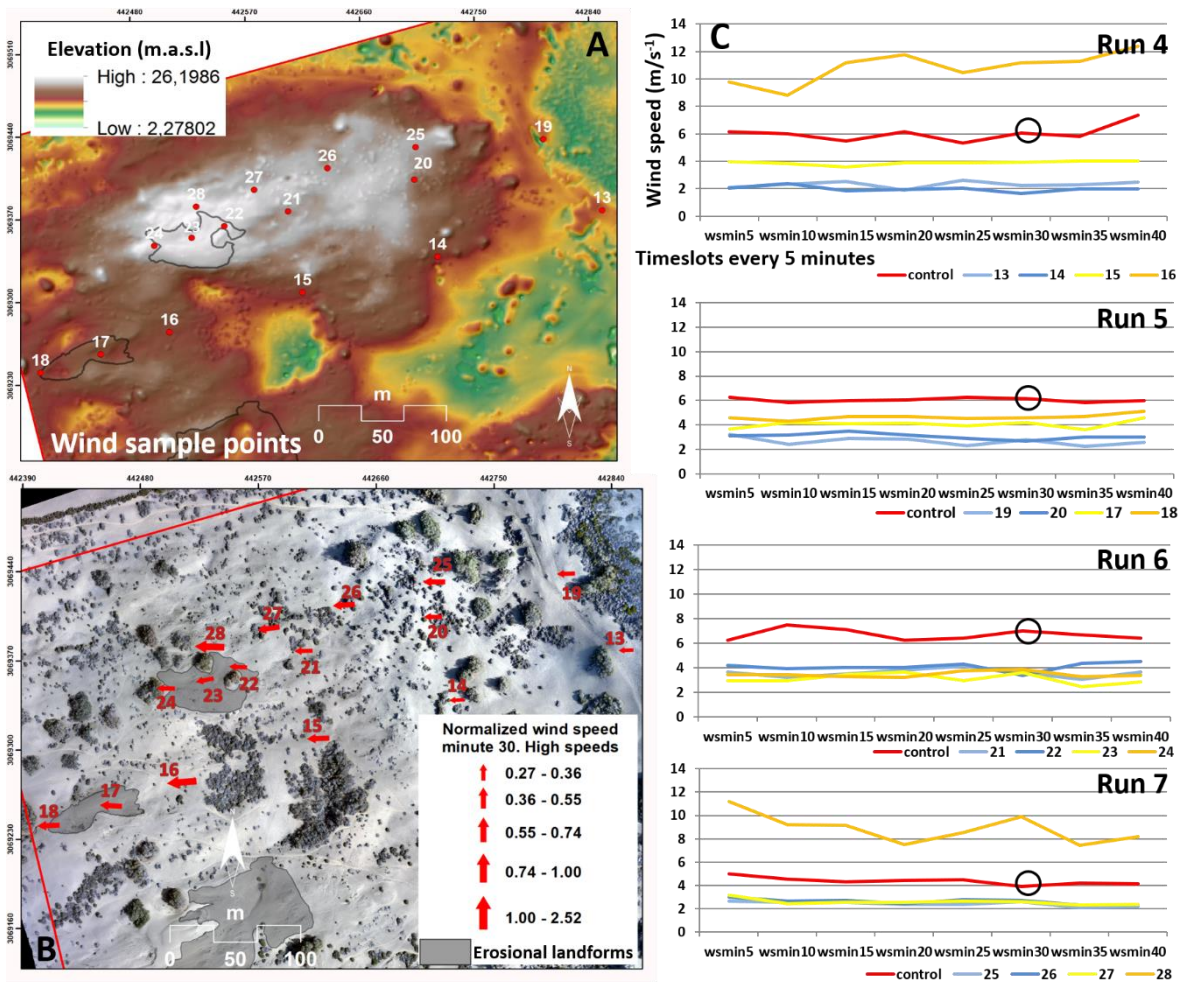
306

307 Figure 6. (A) Position of the sampling points. (B) results of the normalized wind speed (*ASP/ACT*)

308 (minute 30, black circle of the Run`s graphs) with respect to the control tower in each simultaneous

309 sampling. (C) Wind speeds (m s^{-1}) average every 5 minutes in the sampling points on March 25th,

310 2017 (right, Run 4-7).

311 *3.2. PCA Analysis of Vegetation, Wind and Proximity to Infrastructure Data*

312 Table 2 shows significant variables in the first and second components obtained from PCA

313 analyses in each transect. Transect 1 was characterized by variables related to vegetation. Normalized

314 wind data at averages centered in the minutes 20 and 10 (transect 1, day 24th) correlated well with

315 vegetation density (R^2= 0.8774 and 0.777). Although wind is a multifactorial variable, the graph

316 shows that as vegetation density increased, the wind speed decreased. In transect 2 (day 24th), the

317 averages centered in minutes 20 and 10 showed a higher correlation with the mean slope of the

318 sampling point taken from the DEM (i.e., with a topographic variable) (R^2= 0.9184 and 0.8393).

319 According to the dispersion graphic (figure 7, B), the steeper the slope, the lower the wind speed.

320 However, slopes steeper than 5º led to wind acceleration as a result of speed up processes (Garés and

321 Pease, 2015). Transect 3 (day 25th), averages centered in the minutes 30 and 5 were influenced by all

322 variables, although winds were best correlated with slopes (R^2=0.753 and 0.7382). Interestingly, wind

323 speed decreased with increasing slopes on this occasion, with maximum wind acceleration coinciding

324 with average slopes of 5°. In the two last cases (transects 2 and 3), the wind behavior is not

325 aerodynamic related to the mean slope. In transect 2, maybe the answer lies in the next significant

326 variables in the first principal components such as the distance to the buildings, or the elevation, or

327 the combination of both, because in these scatter diagrams, an increase in wind speed is observed.

328 For example in transect 3, the slope also does not show an aerodynamic behavior, because the speed

329 is reduced when the slope increases, but maybe the answer is in the second variable of the first

18

330　principal component (vegetation density), because in this case, maybe the wind at 40 cm height it is

331　being slowed down by the vegetation regardless of whether the slope increases, the scatter diagram

332　is similar to the mean slope. Transect 4 (day 25th), the averages centered in the minutes 30 and 5 were

333　influenced mainly by distance from the resort (R^2= 0.8132 and 0.6718), with increasing wind speeds

334　correlated with increasing distance. The elevation also shows a similar behavior increasing the wind

335　speed, and finally the vegetation density role tends to cushion the wind speed. Finally, transect 5 (day

336　25th) the averages centered in the minutes 30 and 5 were also characterized by altitude (R^2= 0.9983

337　and 0.999), with more wind acceleration at higher elevations. In the scatter diagrams it is possible to

338　observe that as the elevation increases and also the slope increases, the wind speed increases.

339　However, the vegetation density produces a deceleration of the wind if it increases. This last transect,

340　perhaps the least reliable due to the few wind sample points, can affect the statistics, and results in

341　an incomplete understanding of this area of the aeolian shadow zone.

342

343　Table 2. Results of the Principal Components Analysis in each transect using all measured variables

344　and normalized wind speed. Units shown in transect 1.

Variables	Principal Components (minutes 20 and 30)		Principal Components (minutes 10 and 5)	
Transect 1 (minutes 20 and 10)	1	2	1	2
Mean vegetation density (normalized between 0-1)*	-0.907	0.194	-0.898	
Max. Vegetation height (m)*	-0.814	0.345	0.856	
Distance to the urbanization (m)*	0.733	-0.229	-0.801	-0.346
Elevation (m.a.s.l.)	0.358	-0.862	0.333	-0.901
Slope (degree)	0.567	0.711	0.664	0.662
Transect 2 (minutes 20 and 10)	1	2	1	2
Slope*	0.954		0.892	0.359
Distance to the urbanization*	0.915		0.844	0.467
Elevation*	0.803	0.1	0.933	
Max. Vegetation height	-0.693	0.833	-0.521	-0.893
Mean Vegetation density	-0.523	0.712	-0.630	-0.772
Transect 3 (minutes 30 and 5)	1	2	1	2
Slope*	-0.925	0.27	0.915	

19

	1	2	1	2
Mean vegetation density*	-0.811	0.33	-0.892	0.351
Distance to the urbanization*	0.745	0.661	0.765	0.643
Max. Vegetation height	-0.741	0.398	0.439	-0.793
Elevation	0.652	0.73	0.690	0.707
Transect 4 (minutes 30 and 5)	1	2	1	2
Distance to the urbanization*	0.923	0.128	0.899	
Mean vegetation density*	-0.878	-0.363	-0.857	-0.453
Elevation*	0.867	-0.448	0.853	
Slope	-0.129	0.968	-0.651	0.745
Max. Vegetation height	-0.201	0.962	0.670	-0.713
Transect 5 (minutes 30 and 5)	1	2	1	2
Elevation*	0.969		0.968	
Mean vegetation density*	-0.936		-0.933	
Slope*	0.844		0.891	
Max. Vegetation height	-0.878		0.871	
Distance to the urbanization	0.839		0.831	

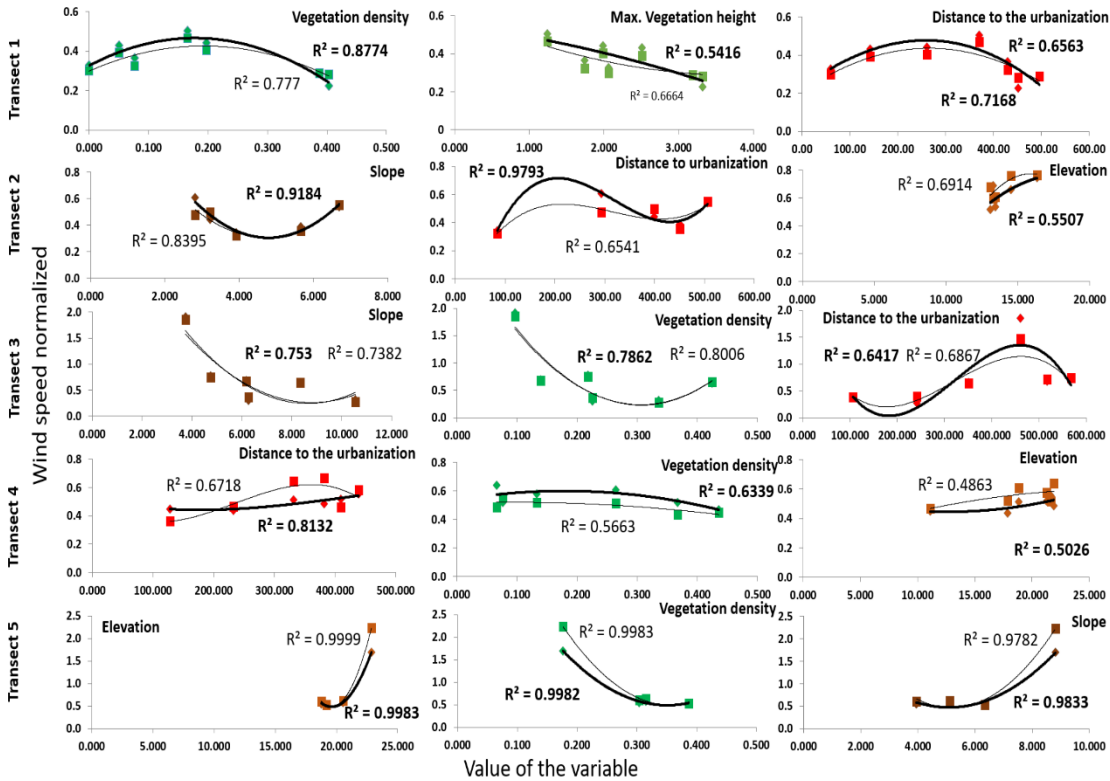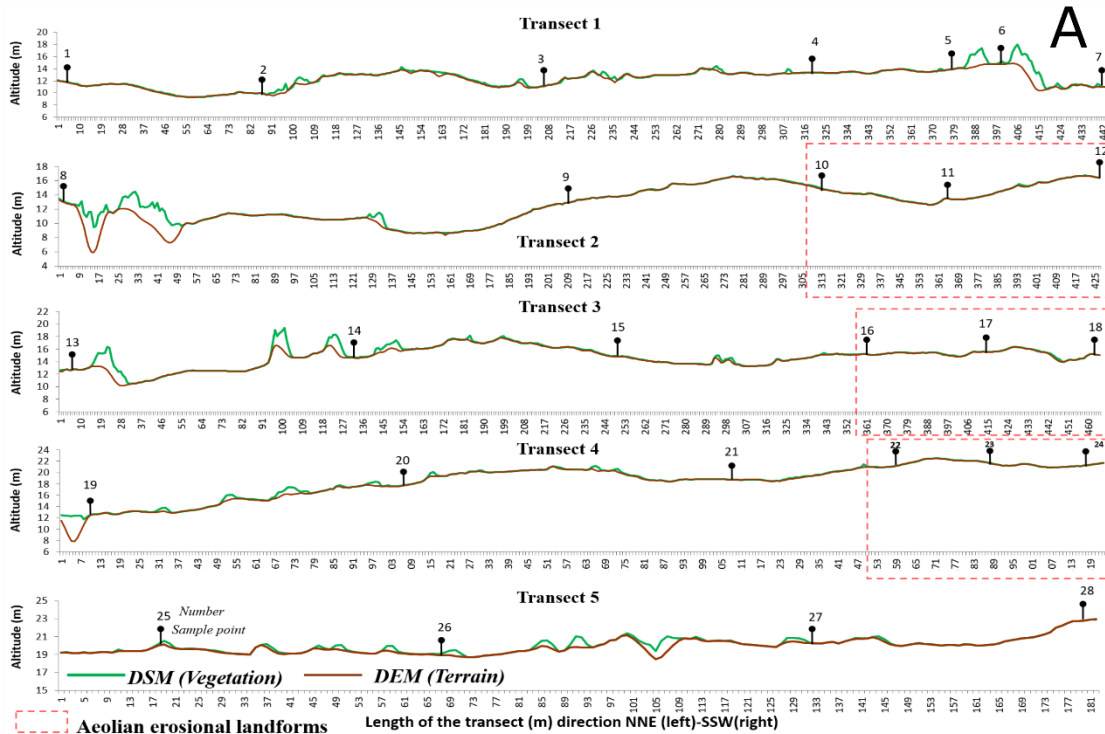* Variables showed in the scatter diagrams of the figure 7

345

346   Overall, transects with no erosional landforms presented a greater influence of vegetation

347   variables on wind speed reduction. In transect 5, elevation had the greatest significant correlation,

348   followed by plant density. In general, winds across transects with erosional landforms (2, 3 and 4)

349   were more affected by variables related to topography. Distance to the resort was significant in all

350   transects, which reinforces the hypothesis that, although the wind speed in this area has been reduced

351   by 50% by urbanizations (Hernández-Calvento et al. al., 2014), there are local wind accelerations

352   (Smith et al., 2017) that result in the formation of erosional landforms. However, this variable in

353   transects 2 and 3 is adjusted with a third polynomial order due to deceleration inside the aeolian

354   erosional landforms 2 and 3. This pattern has also been observed in parabolic dunes and trough

355   blowouts (Hesp and Walker, 2013; Delgado-Fernandez et al., 2018) because under oblique winds, the

356   topography of these aeolian erosional landforms is highly efficient at steering the incoming winds

357   such as the airflow inside the landform becomes parallel to its main axis (Byrne, 1997; Hansen et al.,

358   2009; Hesp & Pringle, 2001; Pease & Gares, 2013). Transect 3 could also be explained by the

359   topographic features and the roughness of the vegetation (Hesp, 1981; Moreno-Casasola, 1986;

360 Mayaud et al., 2016)., In both cases (transects 2 and 3), in the last point of the transect (the end of the

361 erosional landform to the SSW), winds are accelerated facilitating erosion because the airflow is

362 accelerated along the basin toward the depositional lobe, with wind speeds at the crest in this location

363 being roughly double of those measured in the basin (cf. Delgado-Fernandez et al., 2018). These

364 landforms appear at a similar distance from the urbanization (400-500 meters) (García-Romero et al.,

365 2017), suggesting that this is the distance at which wind speeds recover after being decelerated by the
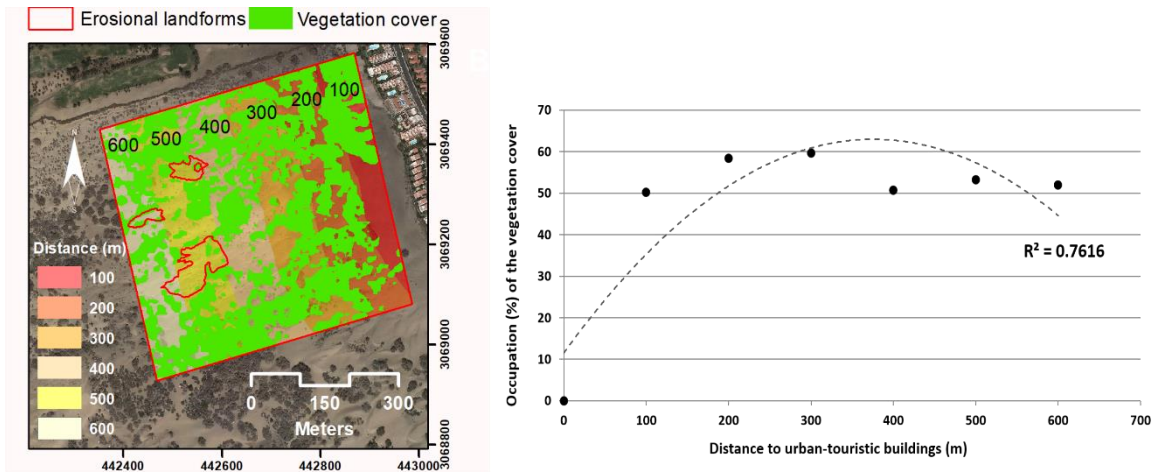
366 urbanization.

367

369   Figure 7. Profiles of the transects studied (DEM and DSM) and the wind sampling points locations

370   (A). Scatter diagrams of the most significant variables obtained by the Principal Components

371   Analysis (B).

372   *3.3. Vegetation role in the aeolian shadow zone*

373   *3.3.1. Distribution of the vegetation cover in the aeolian shadow zone*

374   Increases in vegetation cover were classified into 100 m buffers from buildings (to the northwest of

375   the study site, Figure 8). This allowed exploration of the effect of human activities on vegetation

376   based on the distances to buildings. The vegetation cover continually increases to the southwest from

377   the edge of the buildings, to 400 meters distance. A relationship ($R^2 = 0.7616$) can be observed when

378   only the buildings are considered (figure 8). The results also provide information about the changes

379   experienced by the vegetation in the aeolian shadow area, related to the urban-tourist infrastructures.

380   Actions such as the existence of gardens and its irrigation do occur, as has happened in Argentina or

381   Germany (Grunewald, 2006; Grunewald and Schubert, 2007; Faggi and Dadon, 2010, 2011).

382   However, in the analyses carried out, around 400 meters from the urban-touristic buildings is where

383   less vegetation is concentrated, coinciding with the appearance of the erosional landforms. This is the

384   sector that has experienced the greatest erosion since 1987 (García-Romero et al., 2019). It also

385   coincides with the distance proposed in figure 6 where the wind data analyses indicated that

386   acceleration processes were detected. This reason could be conditioning the non-colonization of

387   plants in this area, and not the presence or absence of water. We must consider that one of the plant

388   communities that have experienced a greater increase in surface in the areas of greater volume of sand

389   is *Cyperus capitatus-Ononis tournefortii* (table 3). It is a strictly psammophilous plant community,

390   so it does not need the existence of a water table (Hernández-Cordero et al., 2015, 2017). In this sense,

391   the hypothesis presented in the previous section is also reinforced, thus justifying an experiment with

392   empirical wind data (speed and direction) and maybe a model derived from them.

393

394   Figure 8. Distribution of the vegetation cover from the urban-tourist buildings to to the southwest of

395   the study area. The relationship between vegetation cover (%) and distance to the urbanization (m) is

396   showed with polynomial (degree 2).

397

398   *3.3.2. Plant communities and their role of the aeolian erosional landforms*

399   Table 3 shows the percent change in plant communities between 2003 and 2017 inside the

400   aeolian erosional landforms area in the study area. In 2003, the erosional landform detected in transect

401   2 (figure 2) was covered by a community of herbaceous plants *Cyperus capitatus-Ononis serrata*

402   (79.95%). Other areas where the vegetation was not detected were classified as null or low vegetation

403   cover (20.04%). In 2017, the plant community *Cyperus capitatus-Ononis serrata* covers 100% of the

404   erosional landform. The only community detected in the erosional landform located in transect 3

405   (figure 2) was also the herbaceous *Cyperus capitatus-Ononis serrata,* both in 2003 and 2017. 44.92%

406   of the aeolian erosional landform in transect 4 (figure 2) was covered by *Cyperus capitatus-Ononis*

407   *serrata* community in 2003, with an increase to 81.03% in 2017. The rest of erosional landform 4

24

408   was not occupied by vegetation in 2003 (55.08%) and in 2017 (18.97%). All erosional landforms

409   were detected in 2003 (García-Romero et al., 2017) but they have evolved in different ways

410   depending on the vegetation cover. Landforms in transects 2 and 4 showed a greater increase in area

411   and eroded volume (García -Romero et al., 2019) because a portion of their surface was not covered

412   by vegetation in 2003 (Table 3). This lack of vegetation favored wind acceleration and sediment

413   erosion. Landform 3 showed greater stability since 2013 due to the presence of vegetation, which

414   reduced wind speeds and prevented strong erosion (Hesp, 1981; Moreno-Casasola, 1986). Note that

415   all landforms showed visible exhumated roots of *Cyperus capitatus-Ononis serrata* (psammophilous

416   perennial rhizomatous forb; psammophilous annual forb) (García-Romero et al., 2019). This is a

417   herbaceous species common in the dune systems of the Canary Islands (Del Arco Aguilar et al., 2010)

418   and a pioneer plant in the colonization of semi-stabilized dunes in the Canaries (Hernández-Cordero

419   et al., 2015), and hence successful at growing in locations with strong sediment transport such as the

420   ones studied here.

421

422   Table 3. Changes of the plant communities between 2003 and 2017 inside the aeolian erosional

423   landforms detected in the study area.

Transect/Erosional landform	Plant communities	%	
		2003	2017
2	C. *Cyperus capitatus-Ononis serrata*	79.95	100
	Null or low vegetation	20.04	0
3	*C. Cyperus capitatus-Ononis serrata*	100	100
4	*C. Cyperus capitatus-Ononis serrata*	44.92	81.03
	Null or low vegetation	55.08	18.97

424

425   In general, the results indicate that the urban-tourist buildings play a predominant role influenecing

426   wind speed patterns over the shadow zone, and that influence is less when incident winds are not

427   across the resort but oblique to it. However, when incident winds flow across the urban-touristic

428 center, an acceleration is detected as the wind moves away from the urbanizations, coinciding with

429 the aeolian erosional landforms detected and with the area where the buildings have lower heights

430 (figure 9). Slower wind speeds in the shadow zone lead to a more rapid vegetation colonization and

431 growth, which in turns plays an important role in decreasing wind speeds and where aeolian erosional

432 landforms are not detected currently.
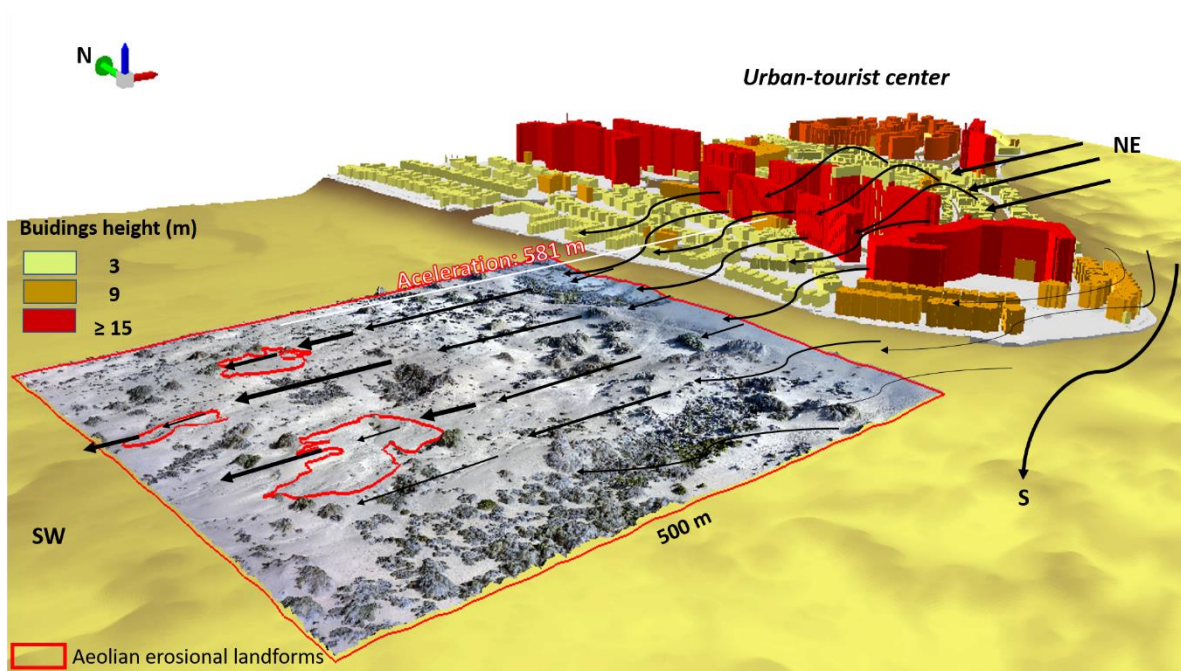
433

434 Figure 9. General scheme of the wind behavior in the aeolian shadow zone crossing the urban-tourist

435 buildings. The thicker the black arrows across the study site (boxed in red) the greater the wind speed.

436

437 **4. Conclusions**

438   This work presents preliminary results from experiments carried out on March 24th and 25th,

439 2017 to study airflow dynamics in an aeolian shadow zone developed as a result of a tourist

440 development in an arid transgressive coastal dune system. Results indicate that: (i) the regional wind

441 direction influences the degree of wind speed change across the study area such that when winds blow

442 across the urban development the wind speed is more affected than when winds blow at an oblique

443 angle or from outside the urbanization; (ii) in general, tourist infrastructure moderately (transect 3) to

444 strongly (transects 4 and 2) influences wind speeds and directions in the study area with PCA

445 correlations ranging from 0.7 to 0.9; (iii) vegetation cover and height have a significant influence in

446 some of the transects (transects 1 and 5) and modify the flow fields accordingly. As vegetation density

447 increased, the wind speed decreased.

448 In this aeolian shadow zone, a suite of erosional landforms is present, located at a similar

449 distance from the urban-touristic infrastructure. This could indicate an acceleration or reattachment

450 of the wind at this distance downwind. The simultaneous collection of wind data, topography and

451 vegetation, as well as distances from the urbanizations and the Principal Components Analysis,

452 indicate that the surface wind (at 0.40 m height) accelerates as it moves downwind from the

453 urbanization, with topography and vegetation introducing variations in the local wind speed. These

454 data provide a valuable field data set for validating future numerical modelling using Computational

455 Fluid Dynamics (CFD) tools, which will allow a greater statistical and spatial analyses of wind speed,

456 direction and turbulence, and to better elucidate the reasons for the presence of erosional landforms

457 in this area.

458 The role that the community of herbaceous plants *Cyperus capitatus-Ononis serrata* is

459 playing in this aeolian shadow zone could be a key to the future evolution of this area. So far we know

460 that this community is growing spatially in those places where erosion is taking place. If this continues

461 into the future, this community will possibly minimize the role that these erosional processes may

462 have (cf. Hernández-Calvento et al.,2014; Hernández-Cordero et al., 2015).

463

464 **Acknowledgements**

471

472   **References**

473   Alonso-Bilbao, I., Sánchez-Pérez, I., Rodríguez, I., Pejenaute-Alemán, I., Hernández-Calvento. L.,

474   Menéndez-González, I., Hernández-Cordero, A., Pérez-Chacón, E., 2007. Aeolian dynamic changes

475   due to the obstacle generated by Traganum moquinii. *Conferencia Internacional sobre*

476   *Restauración y Gestión de las Dunas Costeras (ICCD 2007)*. Santander, Spain, pp. 11-18.

477

478   Byrne, M. L. 1997. Seasonal sand transport through a trough blowout at Pinery Provincial Park,

479   Ontario. *Canadian Journal of Earth Sciences*, 34(11), 1460–1466. https://doi.org/10.1139/e17-118

480

481   Cabrera-Vega, L.L., Cruz-Avero, N., Hernández-Calvento, L., Hernández-Cordero, A.I.,

482   Fernández-Cabrera, E., 2013. Morphological changes in dunes as indicator of anthropogenic

483   interferences in arid dune fields. *Journal of Coastal Research,* SI *65*, 1271-1276.

484

485   Chang, Y.C., Habib, A.F., Lee, D. C., Yom, J.H., 2008. Automatic classification of lidar data into

486   ground and non-ground points. *Paper presented at the ISPRS Congress Beijing 2008*, Beijing, China.

487

488   Crutzen, P.J., Stoermer, E.F., 2000. The "Anthropocene". *Global Change Newsletter,* 41, 17-18.

489   Domínguez-Mujica, J., González-Pérez, J. y Parreño Castellano, J.M. (2011): Tourism and human

490   mobility in Spanish Archipelagos. *Annals of Tourism Research*, 38, 586–606.

491

492   Del Arco Aguilar, M.J., González-González, R., Garzón-Machado, V., Pizarro-Hernández, B., 2010.

493   Actual and potential natural vegetation on the Canary Islands and its conservation status. Biodiversity

494   and Conservation 19, 3089–3140

495

496   Delgado-Fernandez, I., Jackson, D. W., Cooper, J. A. G., Baas, A. C., Beyers, J. H., Lynch, K., 2013.

497   Field characterization of three-dimensional lee-side airflow patterns under offshore winds at a beach-

498   dune system. *Journal of Geophysical Research: Earth Surface*, *118*(2), 706-721.

499

500   Delgado-Fernandez, I., Smyth, T. A. G., Jackson, D. W. T., Smith, A. B., Davidson-Arnott, R. G.

501   D., 2018. Event-scale dynamics of a parabolic dune and its relevance for mesoscale evolution.

502   *Journal of Geophysical Research: Earth Surface*, 123. https://doi.org/10.1029/2017JF004370

503

504   Domínguez-Mujica, J., González-Pérez, J., Parreño Castellano, J.M., 2011. Tourism and human

505   mobility in Spanish Archipelagos. *Annals of Tourism Research*, 38, 586–606.

506

507   Faggi AM, Dadon J. 2010. Vegetation changes associated to coastal touristurbanizations.

508   *Multequina*, 19: 53–76.

509

510   Faggi AM, Dadon J. 2011. Temporal and spatial changes in plant dune diversityin urban resorts.

511   *Journal of Coastal Conservervation,* 15: 585–594.

512

513   García-Romero, L., Hernández-Cordero, A.I., Fernández-Cabrera, E., Peña-Alonso, C., Hernández-

514   Calvento, L., Pérez-Chacón, E., 2016. Urban-touristic impacts on the aeolian sedimentary systems of

515   the Canary Islands: conflict between development and conservation. *Island Studies Journal,* 11(1),

516   91-112.

517

518   García-Romero, L., Hernández-Cordero, A.I., Delgado-Fernández, I., Hesp, P.A., Hernández-

519   Calvento, L., Viera-Pérez, M., 2017. Evolución reciente de geoformas erosivas inducidas por impacto

520   urbano turístico en el interior de un sistema de dunas transgresivo árido (Maspalomas, islas Canarias).

521   *Geotemas*, 17, 263-266.

522

523   García-Romero, L., Hernández-Cordero, A. I., Hernández-Calvento, L., Pérez-Chacón, E., González

524   López-Valcarcel, B., 2018. Procedure to automate the classification and mapping of the vegetation

525   density in arid aeolian sedimentary systems. *Progress in Physical Geography: Earth and*

526   *Environment,* 42 (3), 330–351. https://doi.org/10.1177/0309133318776497

527

528   Garcia-Romero, L., Delgado-Fernández, I., Hesp, P. A., Hernández-Calvento, L., Hernández-

529   Cordero, A.I., Viera-Pérez, M., 2019. Biogeomorphological processes in an arid transgressive

530   dunefield as indicators of human impact by urbanization. *Science of the Total Environment*, 650,

531   73-86. https://doi.org/10.1016/j.scitotenv.2018.08.429

532

533   Garés, P.A., Pease, P., 2015. Influence of topography on wind speed over a coastal dune and blowout

534   system at Jockey´s Ridge, NC, USA. *Earth Surface Processes and Landforms*, 40(7), 853-863.

535

536   Grunewald R. 2006. Assessment of damages from recreational activities oncoastal dunes of the

537   Southern Baltic sea. Journal of Coastal Research 22 (5): 1145–1157.

538

539   Grunewald R, Schubert H. 2007. The definition of a new plant diversity index"H´ıdune" for assessing

540   human damage on coastal dunes—derived from theShannon index of entropy H´ı. Ecological

541   indicator 7: 1–21.

542

543   Gundlach, E.R., Siah, S.J., 1987. Cause and Elimination of the Deflation Zones Along the Atlantic

544   City (New Jersey) Shoreline. Coastal Zone'87, 1357-69.

545

546   Hansen, E., DeVries-Zimmerman, S., van Dijk, D., Yurk, B. 2009. Patterns of wind flow and aeolian

547   deposition on a parabolic dune on the southeastern shore of Lake Michigan. Geomorphology, 105(1-

548   2), 147–157. https://doi.org/10.1016/j.geomorph.2007.12.012

549

550   Hernández-Calvento, L., Jackson, D.W.T., Medina, R., Hernández-Cordero, A.I., Cruz, N., Requejo,

551   S., 2014. Downwind effects on an arid dunefield from an evolving urbanised area. *Aeolian Research,*

552   15, 301-309.

553

554   Hernández-Cordero, A.I., Pérez-Chacón Espino, E., Hernández-Calvento, L., 2015. Vegetation,

555   distance to the coast, and aeolian geomorphic processes and landforms in a transgressive arid

556   coastal dune system. *Physical Geography*, 36 (1), 60–83.

557

558   Hernández-Cordero, A.I., Hernández-Calvento, L., Pérez-Chacón Espino, E., 2017. Vegetation

559   changes as an indicator of impact from tourist development in an arid transgressive coastal dune field.

560   *Land Use Policy,* 64, 479-491.

561

562   Hesp, P.A., 1981. The formation of shadow dunes. *Journal of sedimentary and petrology,* 51 (1),

563   101-112.

564

565   Hesp, P. A., Pringle, A. 2001. Wind flow and topographic steering within a trough blowout. Journal

566   of Coastal Research, 34, 597–601. http://www.jstor.org/stable/25736325

567

568   Hesp, P.A., 2002. Foredunes and blowout: initiation, geomorphology and dynamics. *Geomorphology,*

569   48, 245-268.

570

571   Hesp, P. A., Walker, I. J., 2013. Aeolian environments: Coastal dunes. In J. Shroder, N. Lancaster,

572   D. J. Sherman, & A. C. W. Baas (Eds.), *Aeolian geomorphology. Treatise on geomorphology* (Vol.

573   11, pp. 328–355). San Diego, CA: Academic Press

574

575   Jackson, M.L., Nordstrom, K.F., 2011. Aeolian sediment transport and landforms in managed coastal

576   systems: a review. *Aeolian Research*, 3 (2), 181-196.

577

578   Mayaud, J. R., Wiggs, G. F., Bailey, R. M., 2016. Characterizing turbulent wind flow around dryland

579   vegetation. *Earth surface processes and landforms 41*(10), 1421-1436.

580

581   Mayaud, J. R., Wiggs, G. F., Bailey, R. M., 2017. A field-based parameterization of wind flow

582   recovery in the lee of dryland plants. *Earth Surface Processes and Landforms 42*(2), 378-386.

583

584   Moreno-Casasola, P., 1986. Sand movement as a factor in the distribution of plant communities in a

585   coastal dune system. *Vegetatio*, 65, 67-76.

586

587   Nordstrom, K.F., McCluskey, J.M., 1984. Considerations for control of house construction in coastal

588   dunes. *Coastal Management,* 12, 385-402.

589

590   Nordstrom, K.F., Jackson, N.L., 1998. Aeolian transport of sediment on a beach during and after

591   rainfall, Wildwood, NJ, USA. *Geomorphology,* 22, 151-157.

592

593   Nordstrom, K.F., 1994. Beaches and dunes of human-anthropized coasts. *Progress in Physical*

594   *Geography,* 18 (4), 497–516.

595

596   Nordstrom, K.F., 2004. *Beaches and dunes of developed coasts*. Cambridge University Press.

597

598   Pease, P., Gares, P. 2013. The influence of topography and approach angles on local deflections of

599   airflow within a coastal blowout. Earth Surface Processes and Landforms, 38(10), 1160–1169.

600   https://doi.org/10.1002/esp.3407

601

602   Smith, A.B., Jackson, D.W.T., Cooper, J.A.G., Hernández-Calvento, L., 2017. Quantifying the Role

603   of Urbanization on Airflow Perturbations and Dunefield Evolution. *Earth´s Future*, 5 (5): 520-539.

604

605   Tsoar, H., Blumberg, D.G., 2002. Formation of parabolic dunes from barchan and transverse dunes

606   along Israel's Mediterranean coast. *Earth Surface Processes and Landforms,* 27, 1147–1161.

607

608   Wiedemann, A.M., Pickart, A.J., 2004. Temperate zone coastal dunes. In: Martinez, M.L., Psuty, N.P.

609   (Eds.), *Coastal dunes. Ecology and Conservation. Ecological Studies*, 171. Springer, pp. 54–65.